Masterthesis:

Direct synthesis of phosphorus-doped graphitic carbon

Emanuel Billeter

Supervisor: Dr. Nicholas P. Stadie
Department of Chemistry & Biochemistry
Montana State University, Bozeman, MT

Prof. Dr. M. Kovalenko
Functional Inorganic Materials Group
Laboratory of Inorganic Chemistry
Department of Chemistry and Applied Biosciences
ETH Zürich

Abstract

A new direct synthesis route to bulk phosphorus-doped graphitic carbon from benzene and phosphorus trichloride is described. The resulting materials, with easily tunable phosphorus content, have been thoroughly characterized in terms of composition, structure and chemical environment of phosphorus. The black metallic flakes exhibit the structural features of nanocrystalline graphite with a phosphorus content up to 20 at% (~PC_5). The phosphorus is present in two forms: as stabilized white phosphorus and incorporated within the graphitic lattice. The surface species are readily oxidized upon exposure to air, whereas the bulk of the material remains unchanged. We foresee several potential applications for such materials in batteries, catalysis, and/or energy conversion devices.

Table of Contents

1 Introduction

Graphite is the stable allotrope of carbon under ambient conditions.[1] Its crystal structure consists of layers of six-membered rings in an AB stacking sequence with weak interlayer forces. Graphite has many interesting properties for a variety of different applications. It is highly resistant to thermal and chemical stress and it is thermally and electrically conductive along the planar layers, but not perpendicular to them. Graphite cleaves cleanly along the basal plane due to the weak interlayer forces. This effect, together with a sublimation point of 3730 °C at atmospheric pressure, is the basis of its use as a dry lubricant. Graphene, a single, pristine graphitic layer of carbon atoms, can be made easily by mechanical exfoliation.[2] Graphite forms many low-stoichiometry, binary intercalation compounds, such as MC_6 and MC_8, among which the intercalant can be any of the alkali metals except sodium.[3] These compounds have become very important as energy storage materials, namely in lithium-ion batteries (LIBs).[4] The average annual production of graphite is estimated to be 1.2 megatons worldwide, according to the US Geological Survey.[5] This number is expected to grow considerably with the onset of mass production of LIBs at the Tesla Inc. Gigafactory, which will use an estimated 100'000 t annually.

Substitutional chemical doping is a simple method to alter the properties of graphite. Nitrogen and boron have been widely investigated as chemical dopants since they have a similar atomic radius to carbon and can influence the electronic properties of graphitic materials without much change in the structure.[6-12] The effects of phosphorus doping on diamond and diamond-like carbon (DLC) films have been studied for almost 30 years using different synthesis methods.[13-18] It was found that small concentrations (< 0.5%) of phosphorus dopant yield polycrystalline, n-type semiconducting diamond films. Materials with higher P/C ratios up to 3:1 were found to be amorphous. This work then brought about theoretical studies on the crystal structure and stability of binary carbon-phosphorus compounds in general, for which no bulk crystalline structure has been discovered. First principles density-functional theory (DFT) calculations predicted the existence of a defective zinc-blende structure of composition P_4C_3 and graphitic structures for P_4C_{3+8n} (n = 1,2,3,4).[19-20]

The lowest energy structure of composition PC_3 was predicted by DFT calculations to be layered (see Figure 9).[21] In that structure, the carbon atoms are trivalent (trigonal planar) and the phosphorus atoms are arranged in a tetrahedron with three P-C bonds and one interlayer P-P bond. The phosphorus bond angles of approximately 109 ° lead to kinks in the layers. Several properties were calculated from these findings: the interlayer distance was estimated to be 2.28 Å (equal to the P-P bond length), the band gap was predicted to be at least 1.51 eV (DFT tends to underestimate band gaps), and the heat of formation (ΔH_f) was calculated to be 2 eV per formula unit (+0.67 eV per atom), which would require formation via a kinetic pathway.

Materials of composition PC have been predicted to exhibit bilayer structures, each alternating layer containing six-membered rings of phosphorus atoms or carbon atoms (see Figure 9).[22] All

of the atoms in this structure are in a tetrahedral bonding geometry with a C-P-C bond angle of 101 °. The sp^3 hybridized carbon atoms form interlayer bonds, creating the bilayered structure.

Phosphorus-doped carbon has been studied for applications mainly as a catalyst for the oxygen reduction reaction (ORR).[23-26] The reduction of molecular oxygen to water is a crucial step in the electrochemical conversion of fuels to produce energy in fuel cells. Phosphorus doping enhances the catalytic activity significantly over undoped catalysts prepared by the same methods. It has also been noted that phosphorus doping suppresses the formation of hydrogen peroxide, an undesirable byproduct of the ORR. The mechanism of catalysis in such materials is not well understood, but it has been suggested that the increase in activity is due to structural defects induced by the dopants, rather than active participation of the dopants in the catalytic process.[27] A thoroughly characterized material (or series of materials) with well-defined phosphorus environments could help to understand this mechanism better.

Phosphorus-doped carbon films have also been subject to investigations as active materials in solar cells.[28] The n-type carbon film was deposited on p-type silicon wafers to create a heterojunction cell. Recently, it was shown that phosphorus-doped graphite obtained via the pyrolysis of 1,2-diphosphinobenzene contained ca. 20 at% of phosphorus.[29] A small fraction thereof was present in the form of white phosphorus (P_4) although the precise nature of the phosphorus environments remained difficult to ascertain. While a large fraction of the phosphorus was found to be bonded to oxygen, the presence of P_4 units gave promise to potential applications in lithium-ion storage, perhaps by conversion to Li_3P.

The goal of the work described herein is to determine the feasibility of a direct (single-step) PC_x synthesis from liquid precursors, thoroughly characterize the resulting product, and optimize the synthesis conditions towards obtaining a well-ordered or crystalline material of tunable composition and/or phosphorus environment. This work is motivated by the fundamental lack of bulk P-C binary compounds and by their several potential applications in future energy storage and conversion processes.

2 Experimental Procedures

2.1 Direct Synthesis of PC_x

The direct synthesis of PC_x is based on a previously reported procedure for the synthesis of bulk graphitic BC_x.[12] In short, the heteroatom dopant (i.e., P) is introduced into a closed reactor containing liquid benzene in the form of its liquid halide (i.e., PCl_3); upon pyrolysis at elevated temperature, the hydrogen halide acts as good leaving group allowing incorporation of the dopant into the structure of the forming graphitic carbon. The amount of each precursor in the initial solution is calculated by eq. 1 for any desired phosphorus to carbon ratio in the final product (for $3 \leq x < \infty$). The byproduct becomes chlorine (Cl_2) instead of hydrogen (H_2) if $x < 3$. The total amount of gaseous byproduct should not exceed 2 mmol to ensure the stability of the quartz reaction tubes used in this work.

$$\frac{x}{6}C_6H_6 + PCl_3 \rightarrow PC_x + 3HCl + \left|\frac{x-3}{2}\right| H_2 \quad (1)$$

Phosphorus trichloride (99%, Sigma Aldrich) and benzene (anhydrous, 99.8%, Sigma Aldrich) were charged into a quartz reaction tube (12-16 x 0.9 cm inner diameter) by a micropipette under argon atmosphere. The tube was closed with a Swagelok ultra-torr adaptor, removed from the glovebox, and placed in liquid nitrogen to solidify the precursor solution. The adaptor was connected to a stainless steel Schlenk line, the tube evacuated to 10^{-2} mbar, and flame-sealed at a pre-prepared neck with an oxy-hydrogen torch.

The sealed quartz reactors were placed in the center of a chamber furnace (Carbolite CWF 12/13) equipped with a programable PID controller (Eurotherm 3216). The furnace was heated to a setpoint (800-1050 °C) along a specified heating ramp (at 0.1-1 °C/min), held at the setpoint for 1-12 h, and then allowed to cool in the closed furnace under no specified ramp. After cooling to below 250 °C, the quartz tubes were removed from the furnace and visually inspected for anomalies. To collect the product, the quartz tubes were scored with a diamond blade and carefully opened in a fume hood (note: fumes and/or flames were commonly observed upon opening). The black metallic flakes were collected on a glass filter frit, washed repeatedly with deionized water and acetone, and then dried at 80 °C. In some cases, the flakes adhered strongly to the quartz surface and could not be rinsed off; the reaction tubes were then filled with 10% HF (aqueous) and left standing for several hours. The flakes were filtered off, washed thoroughly with water and then acetone, and then dried at 80 °C.

2.2 Analytical Methods

2.2.1 Scanning Electron Microscopy

Scanning electron microscopy (SEM) was carried out at the Imaging and Chemical Analysis Laboratory (ICAL) at Montana State University using a JEOL JSM 6100 scanning electron

microscope (SEM) operated in secondary electron imaging (SEI) mode. The electron microscope was equipped with two RÖNTEC XFlash 1000 X-ray detectors for energy dispersive X-ray (EDX) analysis. The as-collected flakes were mounted onto sample holders using adhesive tape.

Ultra-high resolution micrographs were collected using a Zeiss SUPRA 55VP field emission scanning electron microscope (FESEM) with a resolution of < 10 nm.

2.2.2 X-ray Diffraction

Powder X-ray diffraction (XRD) was performed using a Rigaku Ultima IV diffractometer using Cu $K\alpha_1$ radiation with a wavelength of 1.54 Å.

The as-collected flakes were suspended in acetone, sonicated for 5 min at room temperature, and then dried at 80 °C. The powdered sample was placed on a silicon single-crystal (zero background) sample holder. The XRD pattern was collected using Rigakus' PDXL software. The parameters used are shown in Table 1.

Table 1. Typical XRD measurement parameters

Scan range [°]	10-55
Sampling width [°]	0.02
Scan speed [°/min]	5
X-ray voltage [kV]	40
X-ray current [mA]	40

2.2.3 Raman Spectroscopy

Raman spectroscopy was performed in backscattering geometry using a Renishaw inVia Raman microscope with an Ar-ion laser (λ = 514 nm). The as-collected flakes were placed on a glass slide under the microscope objective, and care was taken to ensure that the laser beam irradiated the sample surface at a perpendicular angle. At least 2 inter-consistent spectra were collected for each sample in different areas on the sample surface.

2.2.4 Solid-State NMR

Solid-state NMR spectroscopy was performed using a Bruker 11.7 T NMR spectrometer equipped with an Avance III console and a triple resonance 2.5 mm solid state probe head. Experiments were performed at room temperature in static mode or while spinning the sample at 20 kHz magic-angle spinning (MAS) frequency. Chemical shifts were referenced to 85% H_3PO_4 in D_2O for ^{31}P and $Si(CH_3)_4$ for ^{13}C. The number of transients recorded was 2000 for ^{31}P NMR spectra and 16000-24000 for ^{13}C NMR spectra. The classical Hahn echo pulse sequence was used for ^{31}P spectra, and a simple 30°-one-pulse excitation sequence was used for ^{13}C NMR and some ^{31}P NMR spectra. All spectra were acquired without decoupling. The recycle delay was set to 2 s, the

echo delay to 0.1 ms, and the pulse length for 90° flip angle experiments was 5 µs for ^{31}P NMR spectra. A recycle delay of 2 s was used with a 1.7 µs 30° pulse for ^{13}C NMR spectra.

2.2.5 X-ray Photoelectron Spectroscopy

X-ray photoelectron spectroscopy was performed using a PHI 5600 spectrometer using monochromatic Al Kα radiation at 1486.6 eV as an excitation source. The as-collected flakes were pressed into indium foil and inserted into the analysis chamber held at ca. 1.3×10^{-9} mbar. The spectra were recorded at 0.1 eV resolution and analyzed with RBD Instruments' AugerScan software using Gaussian/Lorentzian line shapes and a Shirley background subtraction. Depth profiles were obtained by sputtering the surface of the flakes with a 2 keV Ar^+ ion beam for specified periods of time in between measurements. The XPS data processing and analysis were carried out by M. Nandasiri of the Imaging and Chemical Analysis Laboratory (ICAL) at Montana State University.

3 Results & Discussion

After the synthesis of a new compound or material, thorough characterization of its properties is of utmost importance. In this case, there are three general properties of interest: the chemical composition of samples with different nominal P/C ratios, the lattice structure, and the chemical environment(s) of the constituents, especially of phosphorus.

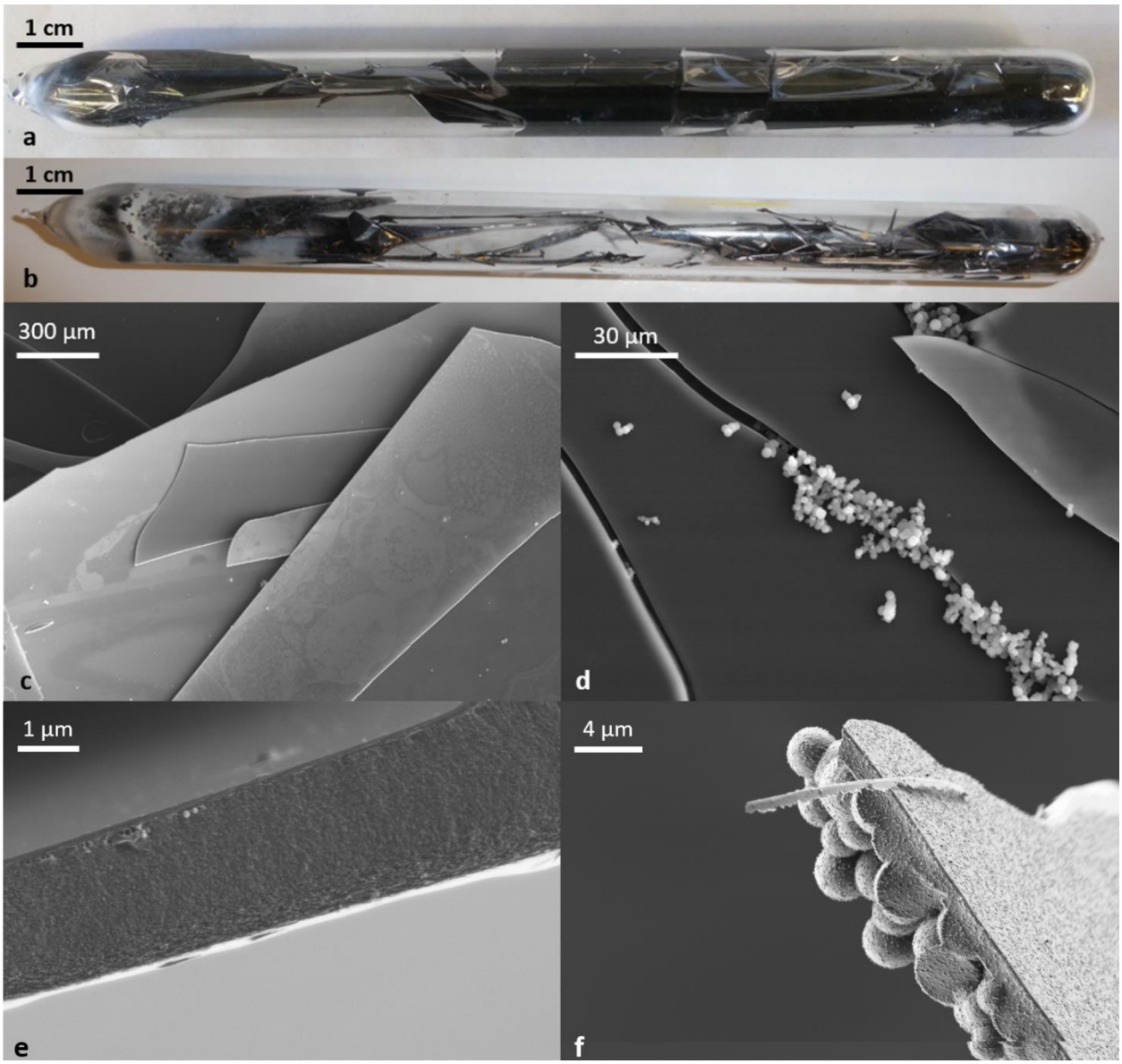

Figure 1. Various photographs (a & b) and electron micrographs (c – f) show PC_x materials under different magnifications. The unopened quartz reactions tubes with black metallic flakes of PC_3 and PC deposited on the walls as well as free standing are shown in a) and b) respectively. Under the electron microscope the flakes have smooth surfaces and edges (c & e) and show some carbon microsphere formation (d & f).

Visual inspection of the quartz reaction tubes immediately after synthesis (before opening) indicates that the product forms as black metallic flakes, both on the quartz walls and within the volume of the tube. The flakes tend to be duller (as opposed to reflective) and more strongly adhered to the walls with decreasing phosphorus content.

Samples with high phosphorus content sometimes show droplets of what appears to be white phosphorus deposited on the inner walls of the reaction tubes before opening (see Figure 10). These samples can ignite spontaneously upon opening and during washing. They also produce a dense white smoke with a garlic-like smell that is characteristic of the oxidation products of white phosphorus.

Inspection of the as-collected flakes of PC_x under electron microscopy reveals mostly even, sheet-like surfaces and various degrees of carbon microsphere formation. The coverage of microspheres can vary from very few (see Figure 1c & d) to total coverage (see Figure 11). It was previously reported, in the synthesis of NC_3 from phenylenediamine, that the formation of such microsphere impurities can be suppressed with the use of a slower heating ramp.[10] The same effect was not observed in this work; samples heated at 0.1 °C/min also show various degrees of microsphere coverage. Extended (or protracted) holding time at the ultimate furnace setpoint also does not seem to influence the formation of microspheres. At the time of this report, it is not clear which parameters influence their growth.

3.1 Composition

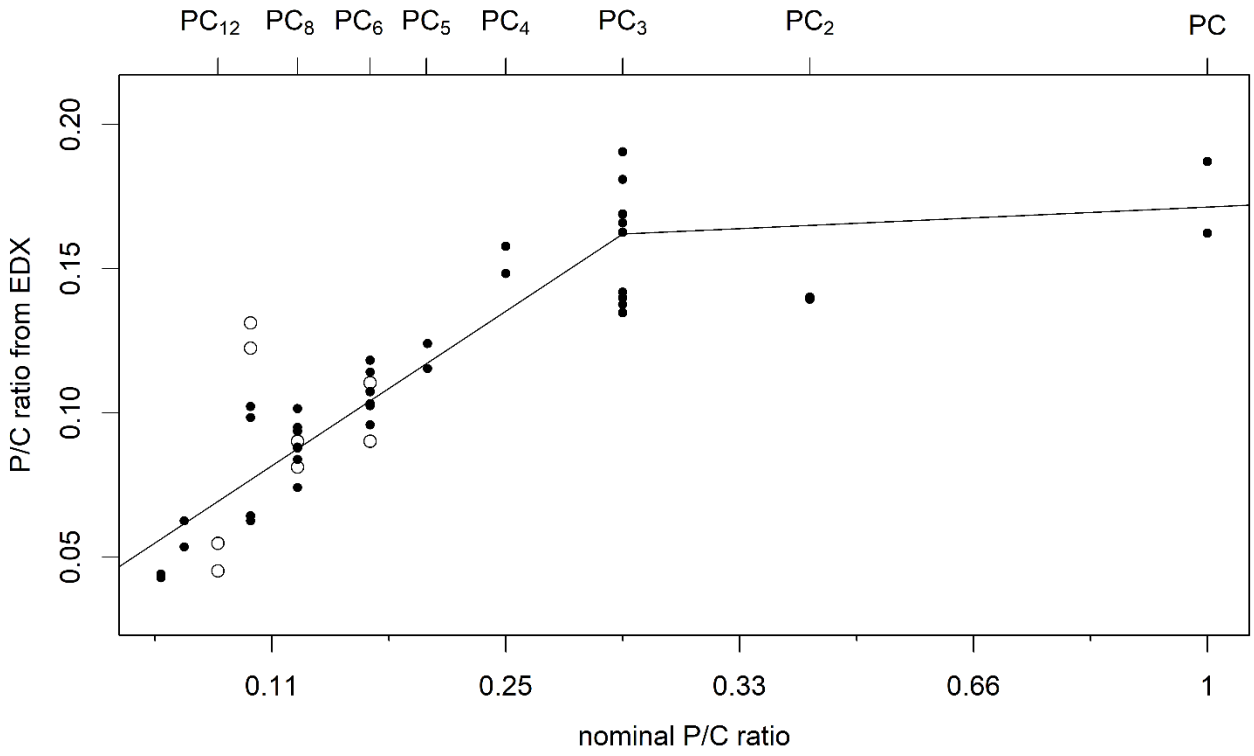

Figure 2. Measured phosphorus to carbon ratio (by EDX analysis) as a function of the nominal P/C ratio (in the precursor mixture). The data suggest a limit of phosphorus incorporation into PC_x at a nominal composition of x = 3. The lines are linear fits from PC_{18} to PC_3 and from PC_3 to PC (in nominal composition). The filled circles indicate samples heated to 800 °C and the unfilled circles indicate samples heated to 1050 °C.

Compositional analysis by energy dispersive X-ray (EDX) spectroscopy shows a wide range of tunable phosphorus content in the directly-synthesized PC_x materials. However, there appears to be an upper limit of phosphorus incorporation at a nominal (precursor) composition of x = 3. When more phosphorus is introduced in the reaction mixture, it is likely to either be oxidized (and volatilized) upon opening the quartz reaction tube, or to be deposited on the tube walls as white phosphorus (see Figure 10) and subsequently washed away during workup. This reasoning is also supported by measurements of the mass of the final yield which can be as high as 98.6% of the starting mass for PC_3 and is generally lower for higher phosphorus-content samples (e.g. 30.4 % for nominal PC). The phosphorus content does not appear to depend on the temperature of synthesis (see Figure 2). Samples with a nominal composition corresponding to $x < 6$ were also prepared at 1050 °C, but they could not be analyzed by EDX spectroscopy due to mechanical issues with the instrumentation.

It should be noted that EDX spectroscopy is not a suitable technique for quantitative compositional analysis since the as-collected flakes must be immobilized on the sample holder using (carbon-based) adhesive tape prior to measurement. This has the effect of reducing the

P/C ratio if the tape is irradiated by the electron beam. The measured P/C ratios in Figure 2 are therefore lower-bound estimates of the actual P/C ratio. However, the extent of this effect remains unknown. There are perhaps two ways to correct these measured compositions. The first would be to measure EDX spectra of standard materials and construct a calibration curve. This is not possible at this time because a pure P-C binary compound does not exist. The second way would be to quantify the relative amounts of phosphorus and carbon by a different analytical method such as a CHN combustion analysis for carbon or phosphate quantification by ion chromatography after the sample is completely oxidized. These analyses are beyond the scope of this project, but could be performed in future work.

Lastly, it should also be noted that EDX spectroscopy is a method for elemental quantification. As used herein, it does not distinguish between different types of chemical environments that exist in this material. The chemical nature of the bonding environments in PC_x materials have instead been analyzed by solid-state NMR spectroscopy and X-ray photoelectron spectroscopy (XPS), as discussed in section 3.3.

3.2 Structure

With the advent of powerful lasers, Raman spectroscopy has become a standard tool for the characterization of carbon based materials.[30-33] Visible wavelength Raman spectroscopy is especially suitable for investigating graphitic materials since it is 50-230 times more sensitive towards sp^2 sites than sp^3 sites, because of the presence of π states. Understanding the Raman spectrum of crystals, e.g., graphite, is simply an exercise in group theory. Understanding the Raman spectrum of even moderately disordered or amorphous materials is not trivial and can require considerable effort.

The Raman spectrum of pristine graphite exhibits two dominant vibrational bands: the intense G band at 1580 cm^{-1} and the second-order 2D band consisting of two components centered around 2700 cm^{-1}.[33] Since the first-order D band is forbidden by symmetry in a perfect crystal of AB-stacked graphite, it can be used as a measure of disorder in graphitic materials. Due to the weak interlayer forces, the Raman spectrum of disordered carbons is dominated by intralayer effects (the interlayer breathing mode is usually found at frequencies below the cutoff of a commercial Raman spectrometer). The D band is very sensitive to stacking disorder in slightly defective samples of crystalline graphite, the D band is weak and consists of a doublet with D_1 and D_2 at 1350 cm^{-1} and 1370 cm^{-1} respectively.[31] With increasing disorder, these bands broaden significantly, become more intense, and overlap to form a single broad peak.

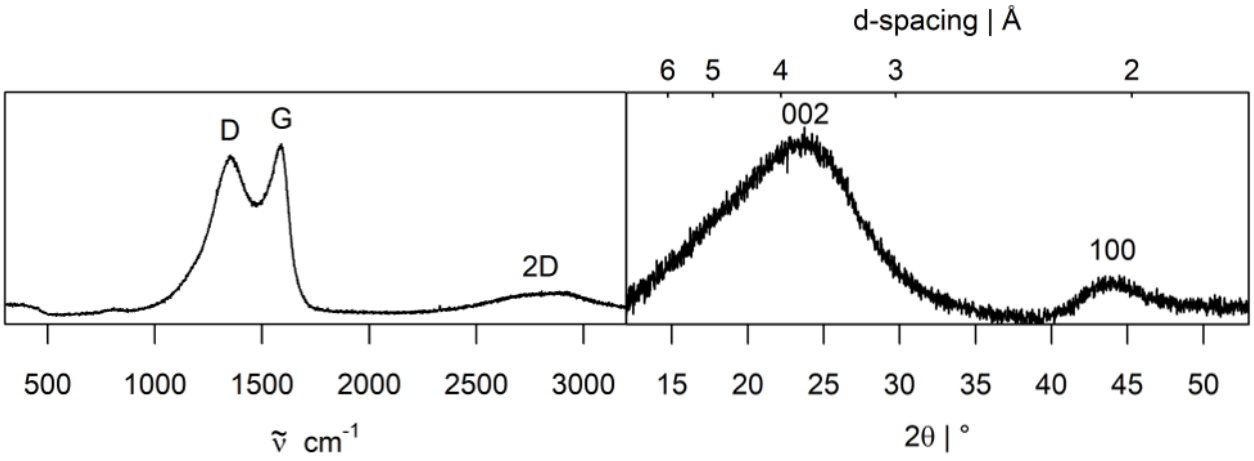

Figure 3. Raman spectrum (left) and XRD pattern (right) of PC_3 synthesize at 800 °C, showing the characteristic features of turbostratic graphite. The Raman spectrum shows broad G and D bands with I_D/I_G ratio of 0.93 and unresolved second order bands around 2800 cm^{-1}. The XRD pattern shows the 002 and 100 reflections corresponding to graphite. The broadness of the 002 refection (FWHM = 11.3 °) is consistent with interlayer disorder. The peak maximum corresponds to an interlayer distance of 3.75 Å, significantly larger than that of graphite (3.35 Å).

Ferrari and Robertson introduced a three-stage model to classify amorphous carbons using Raman spectroscopy.[34] The I_D/I_G ratio and the position of the G band are used to differentiate three phases of amorphization: the first ranging from graphite to nanocrystalline graphite, the second from nanocrystalline graphite to predominantly sp^2 hybridized amorphous carbon, and the third from amorphous carbon to predominantly sp^3 hybridized amorphous diamond. Directly-synthesized PC_3 (at 800 °C) exhibits characteristics from both stage one and two (see Figure 3). The combination of an I_D/I_G ratio of 0.93 and a G band positioned at 1585 cm^{-1} place it within stage one. The unresolved 2D bands that range from 2400 cm^{-1} to 3100 cm^{-1} are typical of stage two. However, it should be noted that the Ferrari and Robertson model is for pure carbons and does not hold to be strictly valid for heavily doped carbons.

X-ray diffraction is an important general tool for structural characterization of materials. In contrast to Raman spectroscopy, X-ray diffraction is very sensitive towards stacking defects. The main characteristics in the XRD patterns of directly synthesized PC_x are the position and width of the 002 reflection. The average interlayer distance (d) is a function of the X-ray wavelength (λ) and the angle of diffraction (θ) according to Bragg's law:

$$n\lambda = 2d \sin\theta \qquad (2)$$

The average d-spacing in the materials investigated herein changes as both a function of phosphorus content and synthesis temperature, as described below.

Peak broadening in XRD can arise from numerous effects such as finite crystallite size and stacking faults. It can also arise from defects and/or a wide distribution of interlayer spacing (disorder). The inclusion of intercalant species within the interlayer galleries is a common cause of increased

interlayer spacing in graphite; we cannot rule out the existence of phosphorus or other species within these galleries. In the case of directly-synthesized PC_x materials, it is not known which effects are the most significant. The peak width is therefore used herein as a general measure for disorder.

3.2.1 Phosphorus Content

Several stochiometric series of PC_x samples were prepared under identical conditions for structural comparison by both Raman spectroscopy and X-ray diffraction. Samples ranging in nominal composition from PC_{12} to PC and synthesized at 800 °C show no change in their Raman spectra, but they do exhibit a significant shift of the 002 peak position from 24.5 ° to 23.7 ° at the transition from PC_5 to PC_4 (see Figure 4). This shift is equivalent to an increase in interlayer spacing from 3.62 Å to 3.75 Å. The peak width also broadens significantly, from 8.8 ° to 11.3 °. There are several possible causes for such a transition to a more disordered lattice with wider interlayer galleries (e.g., the appearance of a new, large intercalant species). The lack of change in the Raman spectrum contains a possible clue; the I_D/I_G ratio in the Raman spectrum is known to be inversely proportional to the in-plane correlation length (L_a) as:[30]

$$\frac{I_D}{I_G} = \frac{C(\lambda)}{L_a} \tag{3}$$

This result, that the correlation length does not change across the transition from PC_5 to PC_4, implies that the differences observed in the XRD patterns between PC_5 and PC_4 are more likely to be caused by changes in the stacking sequence or by the introduction of intercalant species between the layers rather than a decrease in crystallite thickness.

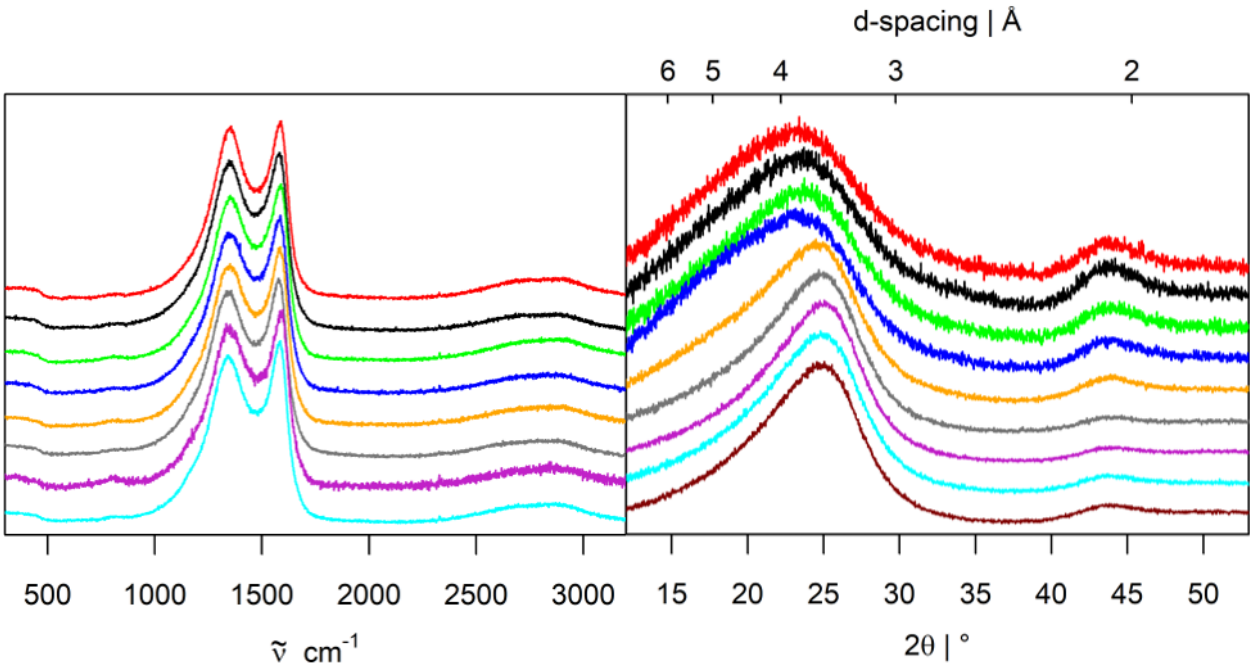

Figure 4. The Raman spectra and XRD patterns of a series of 800 °C PC_x samples showing the influence of phosphorus content on the structure. The Raman spectra remain unchanged with increasing phosphorus content, but there is a clear shift of the 002 XRD reflection between PC_4 and PC_5. This corresponds to an increase in interlayer spacing from 3.62 Å to 3.75 Å. The samples are shown from the top to bottom as: ● PC, ● PC_2, ● PC_3, ● PC_4, ● PC_5, ● PC_6, ● PC_8, ● PC_{10}, ● PC_{12}. All spectra and XRD patterns are normalized to the intensity of the G band or the 002 reflection, respectively.

Compositional analysis using EDX spectroscopy (see Figure 2) showed an upper limit of phosphorus incorporation of ca. 25 at%, after which the average phosphorus content in the resulting material was the same regardless of initial reaction composition. This upper limit is consistent (within experimental error) with the maximum content of phosphorus within the "well-ordered" phase of PC_x (up to ~PC_5) as shown in Figure 4. This implies that PC, PC_2 and PC_3 are much likelier to be disordered and contain large quantities of impurities owing to an excess of volatile (and physically disruptive) chlorine, hydrogen chloride, and other gases in the reaction mixture.

3.2.2 Synthesis Temperature

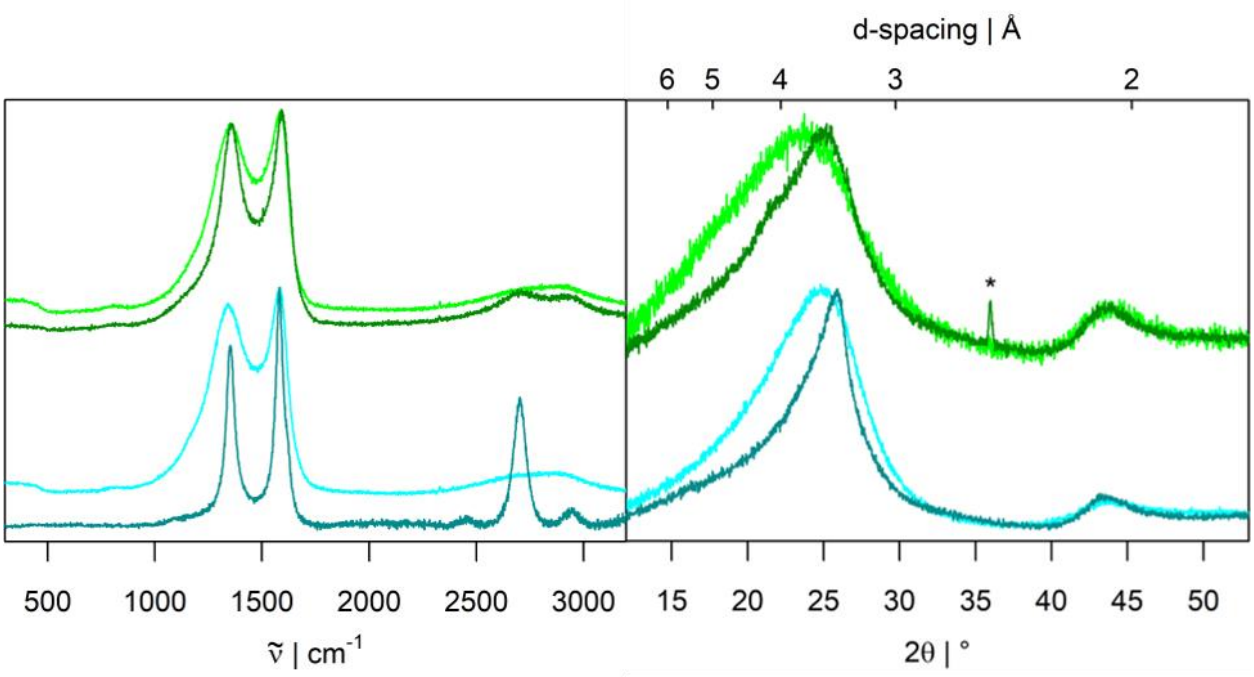

Figure 5. The Raman spectra and XRD patterns of samples heated to 800 °C (light colors) or 1050 °C (dark colors) showing significant differences as a result of increasing synthesis temperature and variations due to differing phosphorus content. Both the Raman and XRD features become narrower with increasing synthesis temperature indicating increased ordering. The asterisk marks a quartz impurity in the XRD pattern. The samples are: ● PC_3 800 °C, ● PC_3 1050 °C, ● PC_{10} 800 °C, ● PC_{10} 1050 °C.

Synthesis temperature plays a very important role in the structure of graphite and graphitic carbon. Graphitic carbons synthesized at 800 °C are considered low-temperature carbons, and are often referred to as either soft or hard carbon depending on whether higher temperature treatments can be performed to recover crystalline graphite. The gold standard for ordered graphite, highly-oriented pyrolytic graphite (HOPG), is produced by stress-annealing at 3000 °C. [35] Polycrystalline graphite is typically obtained at temperatures exceeding 2000 °C. The direct synthesis method used herein (described in Section 2.1) drastically limits the temperature range for the synthesis of PC_x. The closed quartz ampule containing the reaction mixture is susceptible to bursting and eventually melting if heated inappropriately during a reaction. The commonly accepted "softening temperature" of fused silica is ~1680 °C. Since the reactions in this work release a large quantity of gaseous products, the reaction ampule rises to significant pressures during synthesis, and an upper limit of temperature of 1050 °C was used.

Increased synthesis temperature is seen to generally correlate with ordering of the PC_x materials, as can be seen in Figure 5. Samples with less phosphorus content ($x > 3$) exhibit a significantly narrower 002 peak in the XRD pattern with a smaller average interlayer spacing of 3.43 Å. The G and D band in the Raman spectrum are almost baseline separated and the 2D peaks are resolved. All of these features are typical for the first stage in the Ferrari-Robertson model of amorphous

carbons, and therefore these materials can be classified as nanocrystalline. The high phosphorus content samples ($x \leq 3$) show only slightly narrower features as a result of increased synthesis temperature, in both the Raman spectra and the XRD patterns, and a similar decrease in average interlayer spacing to 3.53 Å.

Samples synthesized at 1050 °C are held above the minimum temperature necessary for the reaction for a longer total period of time due to the heating ramp of 1 °C/min. This corresponds to an additional 250 min when the samples are at temperatures above 800 °C, without including the additional cooling time. It is well known that annealing can greatly improve the quality of pure carbon samples[36], but its effect on the chemical purity of the sample (due to possible reactions with the quartz ampule) or on the phase purity of a mixed P-C system remain unknown. To investigate these effects, a series of samples were held at 800 °C for 12 h for comparison. These samples show no significant differences to those held at 800 °C for 1 h (see Figure 12).

3.3 Chemical Environments

The chemical environment of the phosphorus and carbon within directly synthesized PC_x was probed by both solid-state NMR spectroscopy and X-ray photoelectron spectroscopy (XPS). The primary information obtained by NMR experiments is the number and nature of the different phosphorus species that are present within the bulk of the material (see Figure 6). The behavior of the NMR spectrum under different measurement conditions and pulse sequences can also yield structural information (see Figure 7). The nature of the chemical environment of carbon and phosphorus closer to the surface can be probed by XPS analysis, which also yields information about the homogeneity of the chemical environments with respect to depth within the material.

The ^{31}P MAS NMR spectra of PC, PC_3, PC_5, and PC_8 synthesized at 1050 °C all show two signals representative of bulk PC_x, complemented by a third signal in high-phosphorus content samples (see Figure 6). The two common phosphorus environments in every sample are characterized by a sharp signal at -530 ppm that is consistent with the chemical shift of white phosphorus (P_4) and a broad signal corresponding to P-C species centered around 50 ppm.[37] The latter signal is very broad (50kHz). The spectra of PC and PC_3 also contain sharp peaks around 0 ppm that indicate the presence of phosphates. The linewidth of the phosphate (impurity) signals is less than 2 kHz, suggesting that the P-O functionalities are highly mobile species that are not incorporated into the graphitic lattice. The phosphate peaks are only barely detected in PC_5 and are not present in PC_8. The accurate quantification of the phosphate content was not possible in this work owing to instrumental complications concerning tuning the probe head. This is a typical indication of electrically conductive samples for which quantification is impossible.

The presence of white phosphorus (i.e., freely rotating P_4 tetrahedra) after the washing procedure and sample storage in air is a strong indicator that these environments are protected from oxygen by the carbon matrix, perhaps as individual molecules or as small clusters. There is

no indication of any bulk phosphorus phase in either XRD or Raman experiments. It has been previously reported that such stabilized P_4 clusters or domains can incorporate a high content of lithium as Li_3P.[29] Phosphorus is also known to react reversibly with sodium to produce a high-sodium content phase: Na_3P.[38]Combined with the evidence of that these materials are conductors, it is reasonable to suggest that graphitic PC_x materials could be used as alkali-ion battery electrodes.

Further insights into the structure of graphitic PC_x materials were gained by performing ^{31}P NMR spectroscopy under varying conditions (see Figure 7) and analyzing the effect on the P-C resonance at 50 ppm. A spin echo experiment, also called a Hahn echo, was used to reduce homogeneous line broadening resulting from dynamics or relaxation effects.[39] The heterogeneous line broadening, originating from site disorder or chemical shift anisotropy (CSA), is not affected by such an experiment. The spectra collected using a spin echo sequence and a single 30 ° pulse are compared in Figures 7a and 7b; there is no difference in linewidth detected. This implies that the origin of line broadening in the P-C resonance lies in heterogeneous effects. Furthermore, rapid spinning of the sample about the magic angle (54.7 °) can be used to average the contributions from dipolar coupling and CSA.[40-41] The spectra collected under MAS and static conditions are compared in Figures 7b and 7c, respectively; only a small decrease in linewidth is observed. This implies that the main cause of broadening in the P-C resonance lies in site disorder. The results of these experiments can also be used to rule out the presence of red phosphorus, which would also induce a broad signal around 50 ppm.[38, 42] For red phosphorus, however, the broad linewidth is caused by dipolar coupling between the phosphorus nuclei; this coupling would be averaged out during MAS experiments, causing significant narrowing of the signal which was not observed, and thus red phosphorus is unlikely to be present.

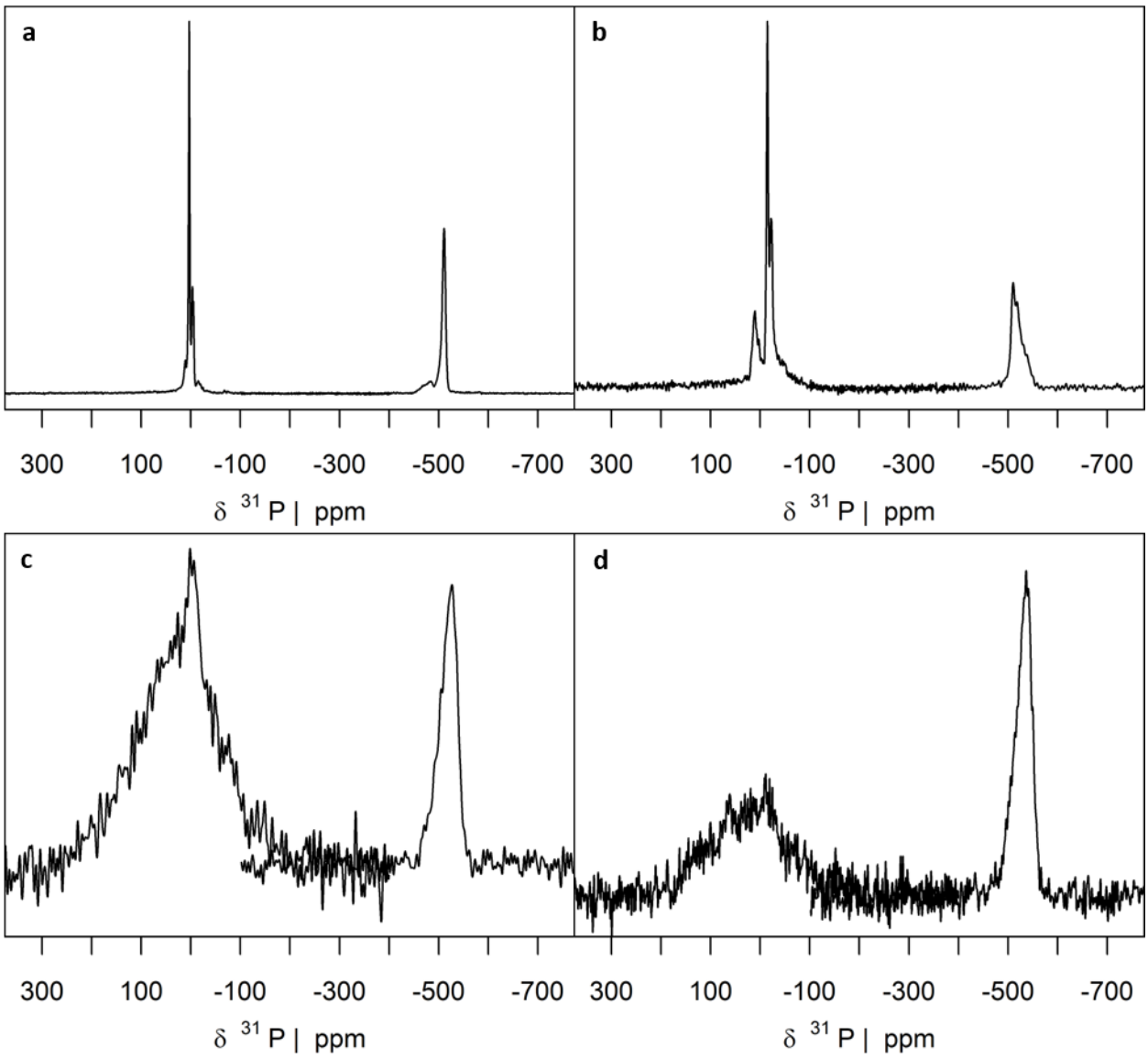

Figure 6. ^{31}P MAS NMR spectra of PC (a), PC_3 (b), PC_5 (c), and PC_8 (d) showing three different phosphorus environments. All samples show a sharp signal corresponding to white phosphorus (P_4) at -530 ppm and a broad signal from 200 ppm to -100 ppm that is attributed to P-C species. The spectra of PC and PC_3 exhibit additional sharp signals around 0 ppm that are characteristic of phosphate species.

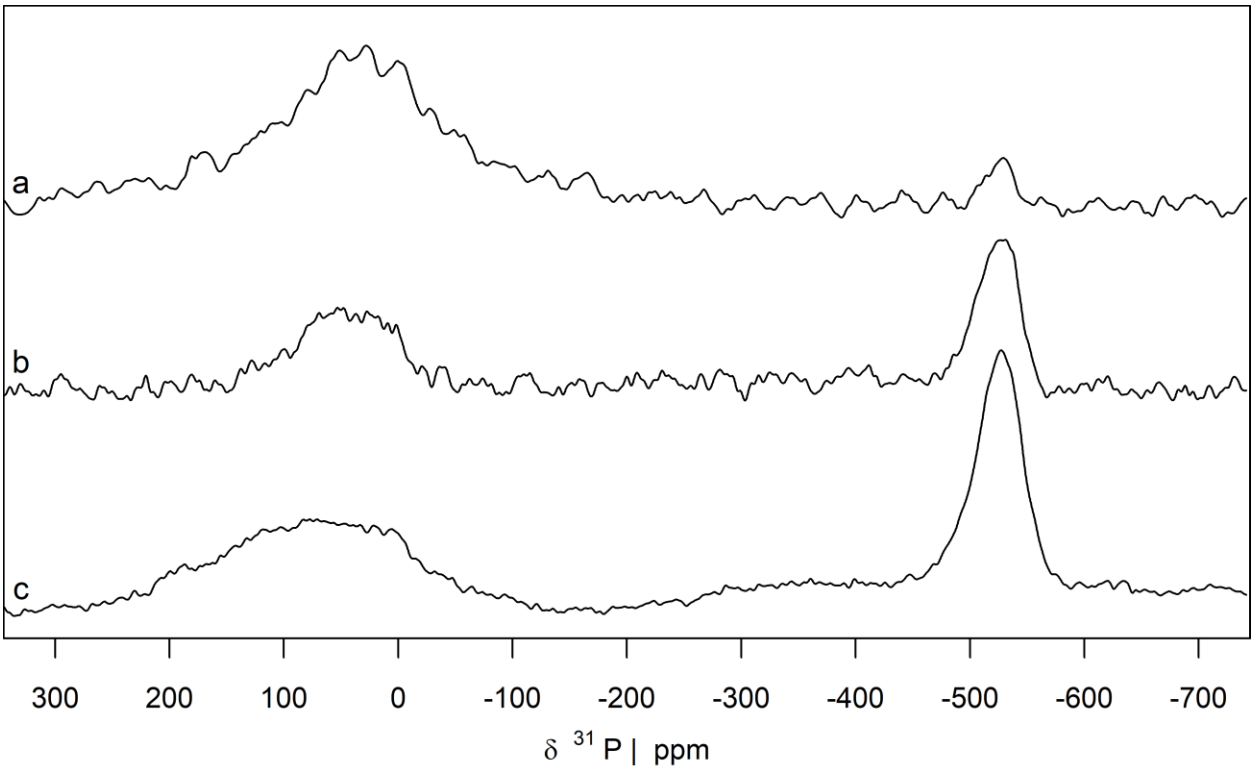

Figure 7. ^{31}P NMR spectra of PC_5 obtained under different experimental conditions, a Hahn echo experiment under 20 kHz MAS (a), a single 30 ° pulse (zg30) under 20 kHz MAS (b), and a single 30 ° pulse (zg30) in static mode (c). The Hahn echo experiment refocuses homogeneous line broadening, and magic angle spinning (MAS) serves to average out any dipolar interactions and chemical shift anisotropy (CSA).

Contrary to NMR, X-ray photoelectron spectroscopy is a surface sensitive method that allows the identification and quantification of different chemical species.[43] In combination with ion beam milling it can also provide a profile of these species as a function of depth. The phosphorus 2p region of the XPS spectra of PC_3 synthesized at 800 °C were measured at three depths: at the surface of the as-synthesized flake, after 2 min of argon sputtering, and after 20 min of argon sputtering, respectively (see Figure 8). Within the deeper bulk of the material (b & c), the phosphorus is mainly present as bonded to other phosphorus (white phosphorus, as indicated by NMR), and some P-C environments are present. Most of the phosphorus directly at the surface, however, is oxidized. This is to be expected since white phosphorus ignites spontaneously in contact with oxygen and trivalent phosphorus incorporated in the graphitic lattice could also oxidize into a pentavalent species. These observations at and just below the surface are consistent with the ^{31}P NMR results, which is a bulk method. Quantification of the relative content of P-P, P-C, and P-O environments is shown in Table 2.

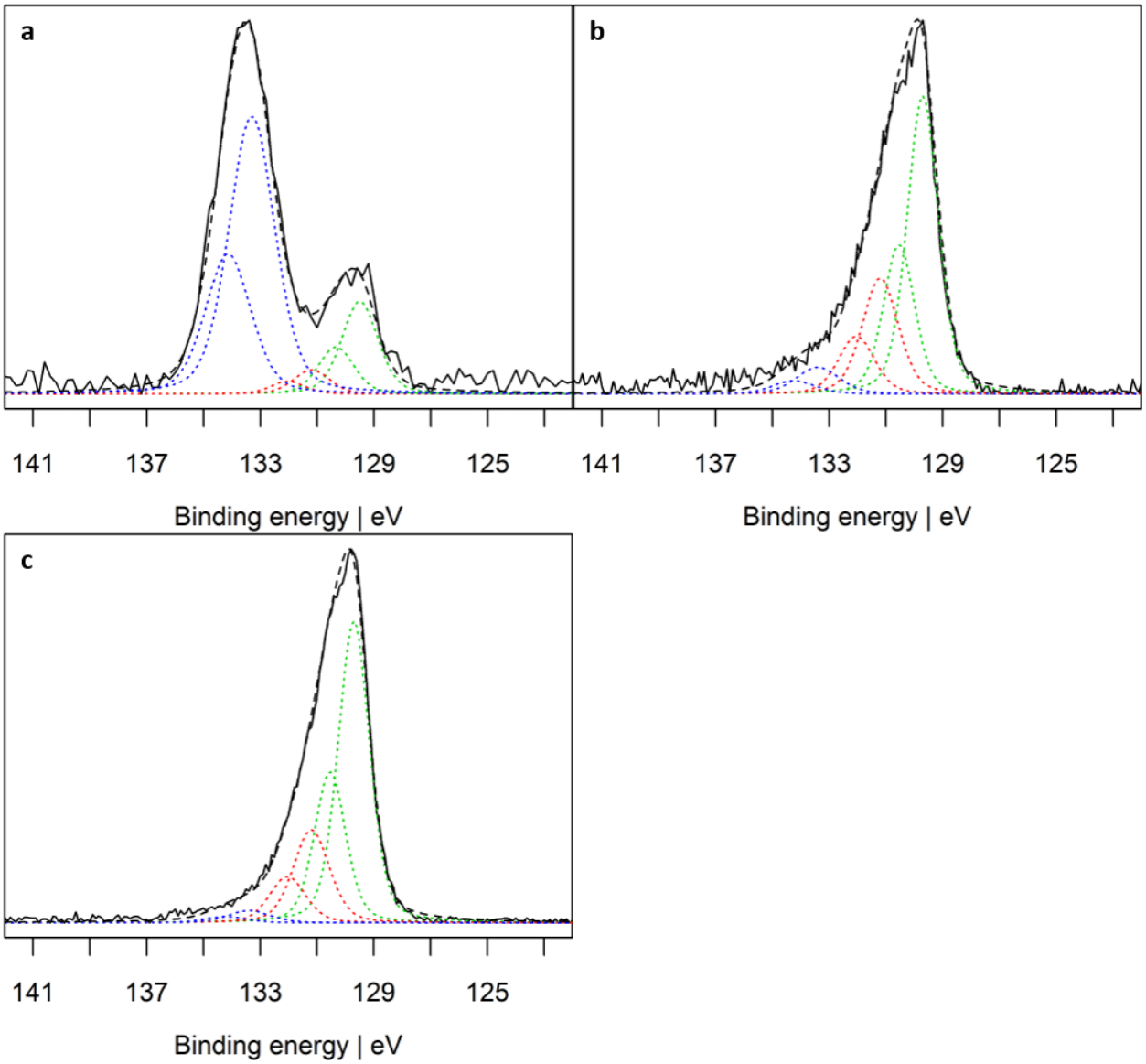

Figure 8. Phosphorus 2p XPS spectra of PC_3 synthesized at 800 °C as a function of depth: at the surface (a), after 2 min Ar-ion beam milling (b), and after 20 min Ar-ion beam milling (c). The solid black line is the measured spectrum, the dashed black line is the sum of all Gaussian fits in blue, red and green, which correspond to P-O, P-C, and P-P bonds, respectively. After only 2 min of ion beam milling, the P 2p spectrum is dominated by P-P environments and the P-O environments become almost negligible.

4 Conclusion & Outlook

The direct synthesis of bulk phosphorus-doped graphitic carbon has been demonstrated. Starting from readily available, cheap liquid precursors, this synthesis method can be used to access a wide range of phosphorus content simply by varying the composition of the initial reaction mixture. The so-obtained, directly-synthesized PC_x materials are dark, conductive flakes with a metallic luster, and exhibit characteristic structural features of nanocrystalline graphite. Compositional studies indicated that a limit of phosphorus incorporation was reached at a nominal composition (initial reaction mixture) corresponding to PC_3. Solid-state NMR experiments revealed the presence of two phosphorus species common to all PC_x compositions: white phosphorus (P_4) molecules or clusters and phosphorus incorporated within the graphitic lattice. Surface analysis using XPS showed that these phosphorus species are significantly oxidized at near the surface of the flake, but remain stable within the bulk of the material even after washing with water and storage in air. The materials produced by the direct method described herein show a significantly lower oxygen content than that of materials prepared from an organic molecular precursor (which is highly sensitive to oxidation and difficult to prepare), while also providing an easily scalable and tunable process.

The presence of stabilized white phosphorus is interesting for battery applications, namely as an anode material for alkali-ion batteries. Bulk white phosphorus is pyrophoric and toxic and therefore considered unsuitable for battery electrodes.[44] Layered black phosphorus suffers from large volume expansion during lithiation/sodiation and poor conductivity.[45] In directly-synthesized PC_x, the graphitic matrix that stabilizes the white phosphorus molecules, clusters, or nanodomains could serve as a conducting framework while mitigating the effects of volumetric expansion upon ion insertion. The materials achieved in this work have already shown to be conductive but the bulk conductivity has yet to be measured.

A further point of interest lies in the fact that phosphorus sites in a graphitic lattice have been shown to enhance the activity of carbon-based ORR catalysts.[23] Their simple synthesis route and wide range of tunable phosphorus content make PC_x materials ideal candidates to understand and optimize this catalytic process. Binary and ternary heteroatom-doped carbons, namely B/N- and B/N/P-doped carbons, have also shown improved catalytic activity over nitrogen-doped carbons for the ORR in acidic media.[46] It was suggested that the presence of electron poor (B) and electron rich (P) sites in the same material could greatly improve the performance of these catalysts. The synthesis route presented herein naturally lends itself to multiple dopants, and early such experiments were carried out in the course of this work. Early results of an XPS study on a material of nominal composition BPC_6 show the presence of both dopants within the bulk of the material.

Future work in this vein should be carried out to improve the crystallinity and chemical composition of the final PC_x material, for which there are several possible routes. Post-synthetic

annealing is often used to improve the structural and chemical regularity of materials. However, there is also the potential to evaporate the elemental phosphorus, even to create highly toxic phosphine gas. Annealing could be performed in vacuum, under high pressure (in a closed reactor), or under gas flow (e.g., hydrogen). Different heating and cooling ramps could also be explored to optimize the crystallization process or to obtain glassy materials. Controlling the synthesis to select for a homogeneous phosphorus environment, either stabilized white phosphorus or phosphorus incorporation within the graphitic lattice, is also of practical and fundamental interest. Lastly, the synthesis of a more crystalline graphitic PC_x material could also serve as the starting point for obtaining tunable, high phosphorus-content graphenes.

It is noteworthy that the presence of sp^3 carbon cannot be excluded on the basis of the materials characterization performed in this work. UV-Raman spectroscopy is, however, a powerful tool to analyze sp^3 carbon, and should be undertaken to address this ambiguity. Such experiments could also yield information as to the dispersion of the G band, which is an important characteristic that could be used to discern between stages 1 and 2 of the Ferrari and Roberson model of the amorphization trajectory of graphitic carbon toward amorphous diamond.

5 Acknowledgements

I would like to thank Dr. Nick Stadie for the opportunity to experience research at Montana State University and for his hospitality. It was very interesting and informative to be part of a brand-new research group on a different continent.

Devin McGlamery recorded all the electron microscope micrographs and the EDX data. He also showed me all the things to do in and around Bozeman, so that I could make the most of my time in Montana.

I would like to thank Prof. Dr. M. Kovalenko for supporting and supervising my master thesis at an external institution and for granting access to the NMR facility.

Marcel Aebli and Laura Piveteau recorded solid-state NMR spectra at the Laboratory for Inorganic Chemistry at ETH Zürich and were extremely helpful for the understanding of their work.

Raman and XRD data were obtained from the Center for Advanced Mineral and Metallurgical Processing (CAMP) at Montana Tech under the supervision of Gary Wyss. I would like to thank him for the access to the instruments and the guidance on how to use them.

6 References

1. Shabalin, I. L., Carbon (Graphene/Graphite). In *Ultra-High Temperature Materials I: Carbon (Graphene/Graphite) and Refractory Metals*, Springer Netherlands: Dordrecht, 2014; pp 7-235.
2. Novoselov, K. S.; Geim, A. K.; Morozov, S. V.; Jiang, D.; Zhang, Y.; Dubonos, S. V.; Grigorieva, I. V.; Firsov, A. A., Electric field effect in atomically thin carbon films. *Science* **2004,** *306* (5696), 666-669.
3. Dresselhaus, M. S.; Dresselhaus, G., Intercalation compounds of graphite. *Advances in Physics* **2002,** *51* (1), 1-186.
4. Armand, M.; Tarascon, J. M., Building better batteries. *Nature* **2008,** *451*, 652.
5. Olson, D. W., USGS Mineral Comodities Summaries, Graphite. Survey, U. S. G., Ed. 2017; pp 74-75.
6. Lowell, C. E., Solid Solution of Boron in Graphite. *J. Am. Ceram. So.c* **1967,** *50* (3), 142-&.
7. Kouvetakis, J.; Kaner, R. B.; Sattler, M. L.; Bartlett, N., A Novel Graphite-Like Material of Composition Bc3, and Nitrogen-Carbon Graphites. *J. Chem. Soc. Chem. Comm.* **1986,** (24), 1758-1759.
8. Kaner, R. B.; Kouvetakis, J.; Warble, C. E.; Sattler, M. L.; Bartlett, N., Boron-carbon-nitrogen materials of graphite-like structure. *Materials Research Bulletin* **1987,** *22* (3), 399-404.
9. Sekine, T.; Kanda, H.; Bando, Y.; Yokoyama, M.; Hojou, K., A graphitic carbon nitride. *Journal of Materials Science Letters* **1990,** *9* (12), 1376-1378.
10. King, T. C.; Matthews, P. D.; Holgado, J. P.; Jefferson, D. A.; Lambert, R. M.; Alavi, A.; Wright, D. S., A single-source route to bulk samples of C3N and the co-evolution of graphitic carbon microspheres. *Carbon* **2013,** *64*, 6-10.
11. King, T. C.; Matthews, P. D.; Glass, H.; Cormack, J. A.; Holgado, J. P.; Leskes, M.; Griffin, J. M.; Scherman, O. A.; Barker, P. D.; Grey, C. P.; Dutton, S. E.; Lambert, R. M.; Tustin, G.; Alavi, A.; Wright, D. S., Theory and Practice: Bulk Synthesis of C3B and its H-2- and Li-Storage Capacity. *Angew. Chem. In.t Edit.* **2015,** *54* (20), 5919-5923.
12. Stadie, N. P.; Billeter, E.; Piveteau, L.; Kravchyk, K. V.; Döbeli, M.; Kovalenko, M. V., Direct Synthesis of Bulk Boron-Doped Graphitic Carbon. *Chemistry of Materials* **2017,** *29* (7), 3211-3218.
13. Okano, K.; Kiyota, H.; Iwasaki, T.; Nakamura, Y.; Akiba, Y.; Kurosu, T.; Iida, M.; Nakamura, T., Synthesis of n-type semiconducting diamond film using diphosphorus pentaoxide as the doping source. *Applied Physics A* **1990,** *51* (4), 344-346.
14. Bohr, S.; Haubner, R.; Lux, B., Influence of phosphorus addition on diamond CVD. *Diam. Relat. Mater.* **1995,** *4* (2), 133-144.
15. Tsang, R. S.; May, P. W.; Ashfold, M. N. R.; Rosser, K. N., Influence of phosphine on the diamond growth mechanism: a molecular beam mass spectrometric investigation1Presented at the Diamond '97 Conference, Edinburgh, Scotland.1. *Diam. Relat. Mater.* **1998,** *7* (11), 1651-1656.
16. Kuo, M. T.; May, P. W.; Gunn, A.; Ashfold, M. N. R.; Wild, R. K., Studies of phosphorus doped diamond-like carbon films. *Diam. Relat. Mater.* **2000,** *9* (3), 1222-1227.

17. Pearce, S. R. J.; May, P. W.; Wild, R. K.; Hallam, K. R.; Heard, P. J., Deposition and properties of amorphous carbon phosphide films. *Diam. Relat. Mater.* **2002,** *11* (3-6), 1041-1046.
18. Fuge, G. M.; May, P. W.; Rosser, K. N.; Pearce, S. R. J.; Ashfold, M. N. R., Laser Raman and X-ray photoelectron spectroscopy of phosphorus containing diamond-like carbon films grown by pulsed laser ablation methods. *Diam. Relat. Mater.* **2004,** *13* (4), 1442-1448.
19. Claeyssens, F.; Allan, N. L.; May, P. W.; Ordejón, P.; Oliva, J. M., Solid phosphorus carbide? *Chem. Commun.* **2002,** (21), 2494-2495.
20. Claeyssens, F.; Oliva, J. M.; May, P. W.; Allan, N. L., Binary phosphorus-carbon compounds: The series P4C3+8n. *International Journal of Quantum Chemistry* **2003,** *95* (4-5), 546-553.
21. Claeyssens, F.; Fuge, G. M.; Allan, N. L.; May, P. W.; Ashfold, M. N. R., Phosphorus carbides: theory and experiment. *Dalton Transactions* **2004,** (19), 3085-3092.
22. Claeyssens, F.; Fuge, G. M.; Allan, N. L.; May, P. W.; Pearce, S. R. J.; Ashfold, M. N. R., Phosphorus carbide thin films: experiment and theory. *Appl. Phys. A* **2004,** *79* (4-6), 1237-1241.
23. Liu, Z. W.; Peng, F.; Wang, H. J.; Yu, H.; Zheng, W. X.; Yang, J., Phosphorus-doped graphite layers with high electrocatalytic activity for the O2 reduction in an alkaline medium. *Angew. Chem. Int. Ed.* **2011,** *50* (14), 3257-61.
24. Liu, Z. W.; Peng, F.; Wang, H. J.; Yu, H.; Zheng, W. X.; Wei, X. Y., Preparation of phosphorus-doped carbon nanospheres and their electrocatalytic performance for O-2 reduction. *J. Nat. Gas Chem.* **2012,** *21* (3), 257-264.
25. Yang, D.-S.; Bhattacharjya, D.; Inamdar, S.; Park, J.; Yu, J.-S., Phosphorus-Doped Ordered Mesoporous Carbons with Different Lengths as Efficient Metal-Free Electrocatalysts for Oxygen Reduction Reaction in Alkaline Media. *J. Am. Chem. Soc.* **2012,** *134* (39), 16127-16130.
26. Li, R.; Wei, Z.; Gou, X.; Xu, W., Phosphorus-doped graphene nanosheets as efficient metal-free oxygen reduction electrocatalysts. *RSC Advances* **2013,** *3* (25), 9978-9984.
27. Jiang, Y.; Yang, L.; Sun, T.; Zhao, J.; Lyu, Z.; Zhuo, O.; Wang, X.; Wu, Q.; Ma, J.; Hu, Z., Significant Contribution of Intrinsic Carbon Defects to Oxygen Reduction Activity. *ACS Catalysis* **2015,** *5* (11), 6707-6712.
28. Rusop, M.; Soga, T.; Jimbo, T., Defect studies and photoelectrical properties of phosphorus doped amorphous carbon films. *Diam. Relat. Mater.* **2004,** *13* (11), 2197-2202.
29. Matthews, P. D.; King, T. C.; Glass, H.; Magusin, P. C. M. M.; Tustin, G. J.; Brown, P. A. C.; Cormack, J. A.; García-Rodríguez, R.; Leskes, M.; Dutton, S. E.; Barker, P. D.; Grosche, F. M.; Alavi, A.; Grey, C. P.; Wright, D. S., Synthesis and extensive characterisation of phosphorus doped graphite. *RSC Adv.* **2016,** *6* (67), 62140-62145.
30. Tuinstra, F.; Koenig, J. L., Raman Spectrum of Graphite. *The Journal of Chemical Physics* **1970,** *53* (3), 1126-1130.
31. Vidano, R. P.; Fischbach, D. B.; Willis, L. J.; Loehr, T. M., Observation of Raman band shifting with excitation wavelength for carbons and graphites. *Solid State Communications* **1981,** *39* (2), 341-344.
32. Lespade, P.; Marchand, A.; Couzi, M.; Cruege, F., Caracterisation de materiaux carbones par microspectrometrie Raman. *Carbon* **1984,** *22* (4), 375-385.

33. Ferrari, A. C., Raman spectroscopy of graphene and graphite: Disorder, electron–phonon coupling, doping and nonadiabatic effects. *Solid State Communications* **2007,** *143* (1), 47-57.
34. Ferrari, A. C.; Robertson, J., Interpretation of Raman spectra of disordered and amorphous carbon. *Physical Review B* **2000,** *61* (20), 14095-14107.
35. Blackman, L. C. F.; Ubbelohde, A. R., Stress recrystallization of graphite. *Proceedings of the Royal Society of London. Series A. Mathematical and Physical Sciences* **1962,** *266* (1324), 20-32.
36. Ferrari, A. C.; Kleinsorge, B.; Morrison, N. A.; Hart, A.; Stolojan, V.; Robertson, J., Stress reduction and bond stability during thermal annealing of tetrahedral amorphous carbon. *Journal of Applied Physics* **1999,** *85* (10), 7191-7197.
37. Kühl, O., *Phosphorus-31 NMR Spectroscopy: A Concise Introduction for the Synthetic Organic and Organometallic Chemist*. 2009; p 1-131.
38. Ramireddy, T.; Xing, T.; Rahman, M. M.; Chen, Y.; Dutercq, Q.; Gunzelmann, D.; Glushenkov, A. M., Phosphorus-carbon nanocomposite anodes for lithium-ion and sodium-ion batteries. *Journal of Materials Chemistry A* **2015,** *3* (10), 5572-5584.
39. Hahn, E. L., Spin Echoes. *Physical Review* **1950,** *80* (4), 580-594.
40. Andrew, E. R.; Bradbury, A.; Eades, R. G., Nuclear Magnetic Resonance Spectra from a Crystal rotated at High Speed. *Nature* **1958,** *182*, 1659.
41. Lowe, I. J., Free Induction Decays of Rotating Solids. *Physical Review Letters* **1959,** *2* (7), 285-287.
42. Bytchkov, A.; Fayon, F.; Massiot, D.; Hennet, L.; Price, D. L., 31P solid-state NMR studies of the short-range order in phosphorus-selenium glasses. *Physical Chemistry Chemical Physics* **2010,** *12* (7), 1535-1542.
43. Watts, J. F.; Wolstenholme, J., Electron Spectroscopy: Some Basic Concepts. In *An Introduction to Surface Analysis by XPS and AES*, John Wiley & Sons, Ltd: 2005; pp 1-15.
44. Sun, J.; Lee, H.-W.; Pasta, M.; Yuan, H.; Zheng, G.; Sun, Y.; Li, Y.; Cui, Y., A phosphorene–graphene hybrid material as a high-capacity anode for sodium-ion batteries. *Nature Nanotechnology* **2015,** *10*, 980.
45. Sun, J.; Zheng, G.; Lee, H. W.; Liu, N.; Wang, H.; Yao, H.; Yang, W.; Cui, Y., Formation of stable phosphorus-carbon bond for enhanced performance in black phosphorus nanoparticle-graphite composite battery anodes. *Nano Lett* **2014,** *14* (8), 4573-80.
46. Choi, C. H.; Park, S. H.; Woo, S. I., Binary and Ternary Doping of Nitrogen, Boron, and Phosphorus into Carbon for Enhancing Electrochemical Oxygen Reduction Activity. *ACS Nano* **2012,** *6* (8), 7084-7091.
47. Naumkin, A. V.; Kraut-Vass, A.; Gaarenstroom, S. W.; Powell, C. P., NIST X-ray Photoelectron Spectroscopy Database. National Institute of Standarts and Technology: 2012; Vol. 4.1.
48. Goodman, N. B.; Ley, L.; Bullett, D. W., Valence-band structures of phosphorus allotropes. *Physical Review B* **1983,** *27* (12), 7440-7450.

7 Appendix

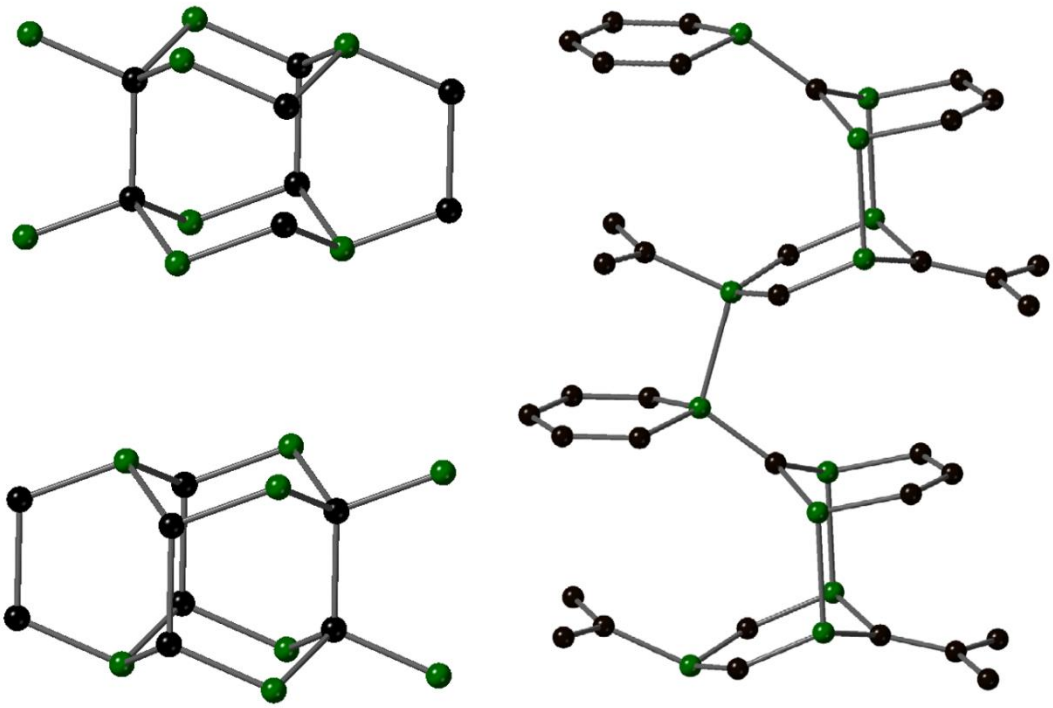

Figure 9. Previously reported lowest energy structures of PC (left) and PC_3 (right).[21] Four unit cells are shown of the bilayer structure of PC with four carbon atoms and four phosphorus atoms each. Two unit cells are shown of PC_3, which exhibits a layered structure with interlayer P-P bonds.

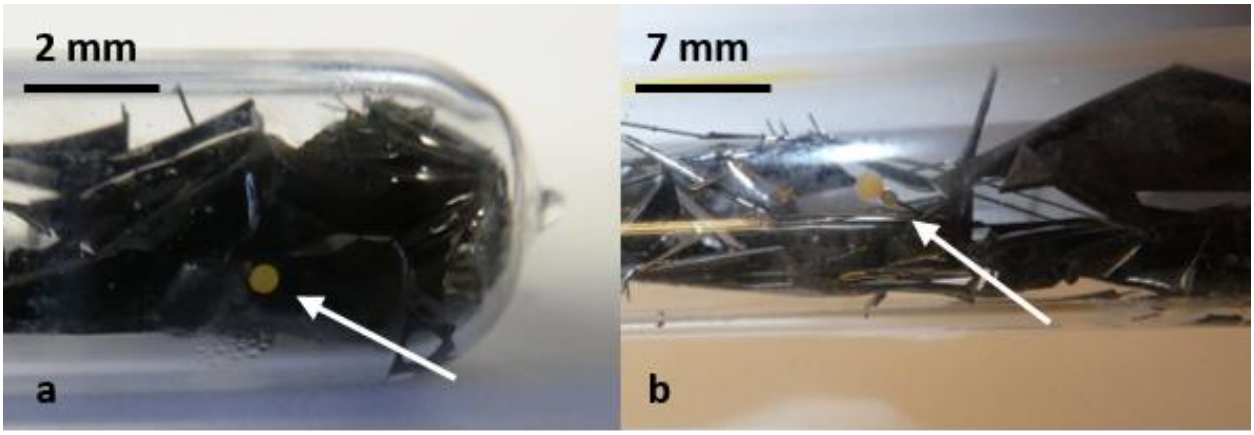

Figure 10. Deposits of white phosphorus (P_4) on the walls of the quartz reaction tubes (indicated by white arrows). Both samples were prepared from a reaction mixture that contained a 1:1 ratio of phosphorus and carbon. Upon opening of the reaction tubes, these droplets ignited and produced a dense white smoke with a characteristic odor of garlic.

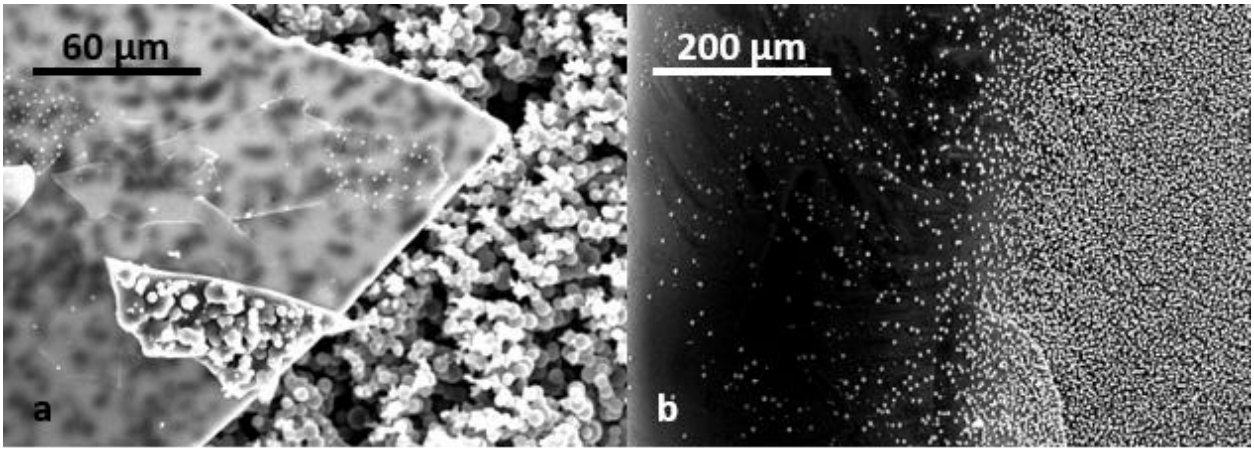

Figure 11. Various degrees of carbon microsphere formation are observed in samples of directly-synthesized PC_x, even within the same sample (a) or on the same flake (b). The relative content of microspheres varies greatly from sample to sample, even when synthesized under the same conditions, and it remains unclear which synthesis parameters influence their growth.

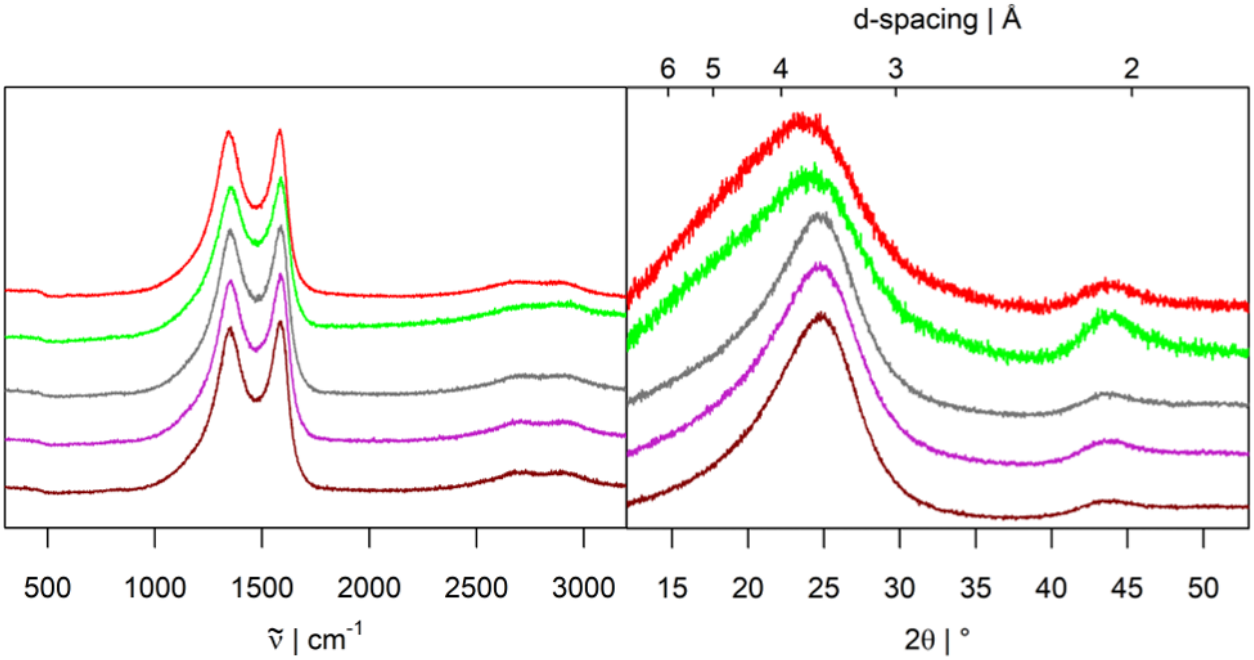

Figure 12. Raman spectra and XRD patterns of a series of PC_x samples synthesized at 800 °C (held at the setpoint for 12 h). There are no significant differences between such samples and those synthesized at 800 °C and held for 1 h. A shift of the 002 reflection in the XRD pattern between PC_3 and PC_6 is similarly observed. The samples shown are ● PC, ● PC_3, ● PC_6, ● PC_8, ● PC_{12}.

Table 2. Quantification of the relative content of the different phosphorus environments shown in Figure 8. The binding energies correspond to the standard values for elemental phosphorus (P-P), triphenylphosphine (P-C), and phosphate (PO_4^{3-}).[47-48] The peak splitting due to spin-orbit coupling was set to 0.84 eV.

Bond type	Binding energy [eV]	Surface (a) [% peak area]	2 min sputtered (b) [% peak area]	20 min sputtered (c) [% peak area]
P-P	129.50	19.8	63.6	70.8
	130.34			
P-C	131.20	5.2	28.5	25.2
	132.04			
P-O	133.30	75	7.9	4
	134.14			